

Mott-Anderson transition in disordered charge-transfer model: Insights from typical medium theory

W. S. Oliveira,^{1,2} M. C. O. Aguiar,^{1,*} and V. Dobrosavljević³

¹*Departamento de Física, Universidade Federal de Minas Gerais, Avenida Antônio Carlos, 6627, Belo Horizonte, Minas Gerais, Brazil*

²*Departamento de Física, Universidade Federal do Piauí, Campus Universitário Ministro Petrônio Portella, Teresina, Piauí, Brazil*

³*Department of Physics and National High Magnetic Field Laboratory, Florida State University, Tallahassee, Florida 32306, USA*

(Received 21 June 2013; revised manuscript received 16 April 2014; published 30 April 2014)

The Mott-Anderson transition in the disordered charge-transfer model displays several new features in comparison to what is found in the disordered single-band Hubbard model, as recently demonstrated by large-scale computational (*statistical* dynamical mean-field theory) studies. Here we show that a much simpler typical medium theory approach (TMT-DMFT) to the same model is able to capture most qualitative and even quantitative aspects of the phase diagram, the emergence of an intermediate electronic Griffiths phase, and the critical behavior close to the metal-insulator transition. The conceptual and mathematical simplicity of the TMT-DMFT formulation thus makes it possible to gain useful new insight into the mechanism of the Mott-Anderson transition in these models.

DOI: [10.1103/PhysRevB.89.165138](https://doi.org/10.1103/PhysRevB.89.165138)

PACS number(s): 71.27.+a, 71.10.Hf, 71.30.+h, 72.15.Rn

I. INTRODUCTION

The physical mechanism behind the metal-insulator transition (MIT) remains one of the basic science questions that still lack complete understanding both on the conceptual and the technical levels. Early work on the subject focused on examining the stability of the metallic phase with respect to weak disorder [1–3] within the framework of a quasiparticle picture and an appropriate generalization [4] of Landau's Fermi liquid theory. These approaches, while formally elegant and appealing, suffer from several conceptual shortcomings that render them of limited relevance to many real materials. Essentially, these treatments describe situations where disorder is viewed as the driving force for the metal-insulator transition and interactions only modify the details of the critical behavior. What is implicitly *assumed* within this picture is that the “host” Fermi liquid is far from any interaction-induced instabilities, where strong correlation effects may destroy [5] the very existence of well-defined quasiparticles. Unfortunately, recent experiments on several model systems, such as two-dimensional electron systems [6] and doped semiconductors [7], have provided evidence that these strong correlation effects may very well be the dominant driving force for electron localization, and thus should be explicitly included in the theory.

Both disorder (Anderson) and correlation (Mott) mechanisms to localization can be treated on the same foot by extensions of dynamical mean-field theory (DMFT) [8]. In the so-called *statistical* DMFT (*statDMFT*) [9] strong correlations are considered in a self-consistent DMFT fashion, while disorder fluctuations are treated by a (numerically) exact computational scheme. Because it is numerically very demanding, this method has been utilized only in a handful of theoretical studies of the Mott-Anderson transition [9–13]. In particular, two of us have recently used it to study the precise form of quantum criticality of the charge transfer model [14]. A much simpler approach—the combination between

typical-medium theory (TMT) [15] and DMFT—provided the first self-consistent description of the Mott-Anderson transition, and offered some insight into its critical regime [16,17]. When applied to the Hubbard model, for weak to moderate disorder TMT-DMFT found a transition closely resembling the clean Mott point, while only at stronger disorder Anderson localization modified the critical behavior [16,17]. Here, we employ TMT-DMFT to solve the charge transfer model, obtaining results in surprisingly good agreement with those recently obtained by us [14] within the more sophisticated *statDMFT* method.

Besides describing the MIT, in this work we also address the electronic Griffiths phase with non-Fermi liquid behavior, which is experimentally observed in heavy fermion systems [18,19], as well as in doped semiconductors [20]. In these systems, the susceptibility is seen to diverge in a power-law fashion in the low temperature limit, not only in the insulating phase, but also in the metallic side of the MIT [21]. In a number of systems, it is the disorder that is responsible for this non-Fermi liquid behavior [5]. Theoretically, this phase is “naturally” incorporated in the description given by *statDMFT* [22]. Within the DMFT framework, it can be addressed by considering the effective model proposed by the authors of Ref. [23]. By combining this last model with TMT, we are able to confirm that for the CT model a Griffiths phase is observed in the region just preceding the correlation-induced MIT, as within *statDMFT* [14].

In the present work, we consider the charge transfer (CT) model because it can describe the systems of our interest better than the single-band Hubbard model. This is the case since the first of these gives a more realistic description of spatial charge redistribution as the MIT is approached, which is important because local correlation effects strongly depend on orbital occupation. In this context, it is interesting to note that the CT model phase diagram seems to differ from that of the single-band Hubbard, even in qualitative aspects [14]. Moreover, when both DMFT and TMT-DMFT are applied to the Hubbard model, the cavity field does not fluctuate, meaning that important fluctuation effects associated with the Griffiths phase and the precise nature of quantum criticality are ignored.

*Corresponding author: aguiar@fisica.ufmg.br

In contrast, when the same method is used to solve the CT model a degree of fluctuation is retained, according to the effective model cited above [23], hence even the simplified theories capture effects such as the Griffiths phase. Another advantage of considering the CT model is that its standard formulation uses the $U = \infty$ constraint for the correlated band, allowing a simpler large N (slave boson) solution [24], which is not available for finite U Hubbard models.

As mentioned above, to solve the disordered CT model in this paper we use the TMT-DMFT method, which allows a detailed description of the system close to the MIT because of its conceptual and mathematical simplicity. According to our current results, as the interaction-induced transition is approached, a fraction of sites turn into local moment, but *not all* of them do it. This is in contrast to the TMT-DMFT results for the Hubbard model [17] where *all* sites turn into local moments close to the Mott transition. The phase diagram for the CT model thus includes a *disordered* Mott insulating phase, which is qualitatively different than the Mott insulator observed for the Hubbard model. The disorder-induced MIT is also qualitatively different than for the Hubbard model. For the CT model most of the sites Anderson-localize, but *none* of them turn into a local moment as disorder increases. In the case of the Hubbard model, we have a two-fluid picture, where a fraction of the sites go through Anderson localization, while *the rest* of them Mott-localize [17].

The paper is organized as follows. In the next section we define the model we consider and the method we use to solve it. Section III is devoted to our numerical results. We present our phase diagram, discuss the disorder (Sec. IIIA) and the interaction-induced (Sec. IIIB) transitions, with special emphasis to the behavior of the physical quantities that characterize the transitions, and finally present results related to the Griffiths phase (Sec. IIIC). We end by summarizing our main conclusions.

II. MODEL AND ITS SOLUTION

A. Charge transfer model and TMT-DMFT equations

The CT model is a two band model, where one band represents conduction electrons and the other corresponds to localized or f -type electrons, for which the electron-electron interactions are strong. It has been used to describe various systems, including oxides [25] and doped semiconductors [20]; for the doped semiconductors, the disordered version of the model is the relevant one, which is indeed the problem we address in this paper.

The CT model description of the Mott transition can be understood as follows: In the clean case, the insulating phase is approached as the f -electron energy decreases, which implies in a smaller number of conduction electrons per site; the transition itself takes place when this quantity vanishes. A careful study on the regimes where this model can be used to describe the Mott transition in the clean case can be found in Ref. [26], for example.

In the disordered case, the CT model is given by the disordered Anderson lattice model supplemented by the condition that the average number of electrons on each site is equal to 1. The Hamiltonian for the Anderson lattice

model is

$$H = \sum_{ij\sigma} [(\varepsilon_j - \mu)\delta_{ij} - t]c_{i\sigma}^\dagger c_{j\sigma} + (E_f - \mu) \sum_{j\sigma} f_{j\sigma}^\dagger f_{j\sigma} + V \sum_{j\sigma} (c_{j\sigma}^\dagger f_{j\sigma} + f_{j\sigma}^\dagger c_{j\sigma}) + U \sum_j n_{fj\uparrow} n_{fj\downarrow}, \quad (1)$$

where $c_{j\sigma}^\dagger$ ($c_{j\sigma}$) creates (destroys) a conduction electron with spin σ on site j , $f_{j\sigma}^\dagger$ and $f_{j\sigma}$ are the corresponding creation and annihilation operators for a localized f electron with spin σ on site j , $n_{fj\sigma} = f_{j\sigma}^\dagger f_{j\sigma}$ is the number operator for f electrons, t is the hopping amplitude to nearest neighbors, E_f is the f -electron energy, U is the on-site repulsion between f electrons, V is the hybridization between conduction and f electrons, and μ is the chemical potential. Throughout this paper we use the half-bandwidth for conduction electrons as the unit of energy; the hybridization potential is chosen to be $V = 0.5$.

In Eq. (1), disorder is introduced through the on-site energies ε_j for conduction electrons, which follow a distribution $P(\varepsilon)$. As we want to be able to address the electronic Griffiths phase, we must reserve special attention to the disorder distribution we consider. As we mentioned before, this phase appears naturally when one treats the disordered correlated system through *statDMFT* [22], but this is not necessarily the case when standard DMFT is considered. In this case, it has been shown that essentially all the properties of the electronic Griffiths phase can be described *if* we “correctly” choose the model to study and the disorder distribution [23].

According to the authors of Ref. [23], the recipe to describe the Griffiths phase in a DMFT level is to include in the calculation cavity fluctuations naturally described within *statDMFT*. First, one has to consider a two band model as the CT model we treat here: In this case the bath seen by each impurity problem fluctuates, that is, changes from site to site [see Eq. (4) below]. In addition, the disorder should be present in the on-site conduction electron energy, which necessarily follows a Gaussian distribution. This specific form of disorder generates a distribution of *renormalized* energies, which is also Gaussian, as it is the case when *statDMFT* with *any* disorder distribution of *bare* energies is considered. Following these findings, in this paper we assume a Gaussian form for $P(\varepsilon)$, with zero mean and standard deviation equal to W , to be able to describe the Griffiths phase within TMT-DMFT.

To finish the description of the CT model, we add that the condition that the average number of electrons on each site is equal to 1 can be enforced by adjusting the chemical potential and can be written as

$$\langle n_{cj} \rangle + \langle n_{fj} \rangle = 1, \quad (2)$$

where $n_{fj} = n_{fj\uparrow} + n_{fj\downarrow}$ gives the number of f electrons on site j , $n_{cj} = n_{cj\uparrow} + n_{cj\downarrow}$ is the corresponding number operator for conduction electrons, with $n_{cj\sigma} = c_{j\sigma}^\dagger c_{j\sigma}$, and the averages are taken over the distribution $P(\varepsilon)$.

As anticipated in the Introduction, we use a combination of TMT and DMFT to solve the disordered CT model. Within this combination [15–17], the lattice problem is mapped onto an ensemble of single-impurity problems, corresponding to sites with different values of the local energy ε_j , each

being embedded in a typical effective medium which is self-consistently calculated. In contrast to standard DMFT [27], TMT-DMFT determines this effective medium by replacing the spectrum of the environment (“cavity”) for each site by its typical value, which is determined by the process of *geometric* averaging.

To be more specific, within TMT-DMFT the Hamiltonian of Eq. (1) is mapped onto an ensemble of single-impurity problems, each of which is given by the following action

$$S(j) = \sum_{\sigma} \int_0^{\beta} d\tau \int_0^{\beta} d\tau' f_{j\sigma}^{\dagger}(\tau) [\delta(\tau - \tau') (\partial_{\tau} + E_f - \mu) + \Delta_{fj}(\tau - \tau')] f_{j\sigma}(\tau') + U \int_0^{\beta} d\tau n_{fj\uparrow}(\tau) n_{fj\downarrow}(\tau), \quad (3)$$

where the Fourier transform of $\Delta_{fj}(\tau - \tau')$ satisfies

$$\Delta_{fj}(i\omega) = \frac{V^2}{i\omega + \mu - \varepsilon_j - t^2 G_c^{\text{typ}}(i\omega)}. \quad (4)$$

A Bethe lattice of infinite coordination number was considered when writing the above equation.

$G_c^{\text{typ}}(i\omega)$ is the typical Green’s function for conduction electrons, which within TMT-DMFT is given by the Hilbert transform of $\rho_c^{\text{typ}}(\omega)$, the typical value of the local density of states (LDOS). In the equations, we have

$$G_c^{\text{typ}}(i\omega) = \int_{-\infty}^{\infty} d\omega' \frac{\rho_c^{\text{typ}}(\omega')}{i\omega - \omega'}, \quad (5)$$

where

$$\rho_c^{\text{typ}}(\omega) = \exp\{\langle \ln \rho_{cj}(\omega) \rangle\} \quad (6)$$

and

$$\rho_{cj}(\omega) = -\pi^{-1} \text{Im} G_{cj}(\omega) \quad (7)$$

is the LDOS.

The local Green’s function for conduction electrons appearing in the above equation satisfies

$$G_{cj}(i\omega) = \frac{1}{i\omega + \mu - \varepsilon_j - t^2 G_c^{\text{typ}}(i\omega) - \Phi_j(i\omega)}, \quad (8)$$

where

$$\Phi_j(i\omega) = \frac{V^2}{i\omega + \mu - E_f - \Sigma_{fj}(i\omega)}, \quad (9)$$

and $\Sigma_{fj}(i\omega)$ is the single-impurity self-energy, which is a solution of the action given in Eq. (3).

By looking at Eq. (6), for example, one can conclude that the problem defined by these equations corresponds to a self-consistent calculation. In other words, within TMT-DMFT the conduction electron effective medium seen by each impurity is self-consistently determined.

B. Slave-boson impurity solver

To solve the single-impurity problems of Eq. (3), we use the slave-boson (SB) technique in the $U \rightarrow \infty$ limit [24,28]. In this case, the impurity Green’s function can be

written as

$$G_{fj}(i\omega) = \frac{Z_j}{i\omega - \varepsilon_{fj} - Z_j \Delta_{fj}(i\omega)} \quad (10)$$

$$\equiv Z_j G_{fj}^{\text{QP}}(i\omega), \quad (11)$$

where Z_j is the local quasiparticle (QP) weight and ε_{fj} is the renormalized f -electron energy. These two parameters are obtained by solving the following set of equations

$$2 \int_0^{\infty} \frac{d\omega}{\pi} \text{Re}[\Delta_{fj}(i\omega) G_{fj}^{\text{QP}}(i\omega)] = E_f - \varepsilon_{fj}, \quad (12)$$

$$Z_j + 2 \int_0^{\infty} \frac{d\omega}{\pi} \text{Re}[G_{fj}^{\text{QP}}(i\omega)] = 0. \quad (13)$$

For more details on the $U \rightarrow \infty$ SB treatment we refer the reader to Ref. [29].

Before finishing the section, it is convenient to note that in terms of the two SB parameters Eq. (9) can be rewritten as

$$\Phi_j(i\omega) = \frac{Z_j V^2}{i\omega - \varepsilon_{fj}}. \quad (14)$$

III. NUMERICAL RESULTS

Let us now present and discuss the numerical results we obtained for the CT model using TMT-DMFT. In this section, we also compare these results with those obtained by two of us within the more sophisticated *statDMFT* [14], which provides an exact numerical treatment of localization in the absence of interactions, and reduces to the standard DMFT treatment in the absence of disorder [9].

Figure 1 presents our phase diagram. As we described previously [14], starting from a disordered correlated metal, a transition to a correlated Anderson insulator takes place as disorder increases; on the other hand, a disordered Mott insulating phase is observed for large values of the CT energy. This energy is defined as $E_{ct} = -E_f$ and plays the role of the interaction energy U in the Hubbard model. By

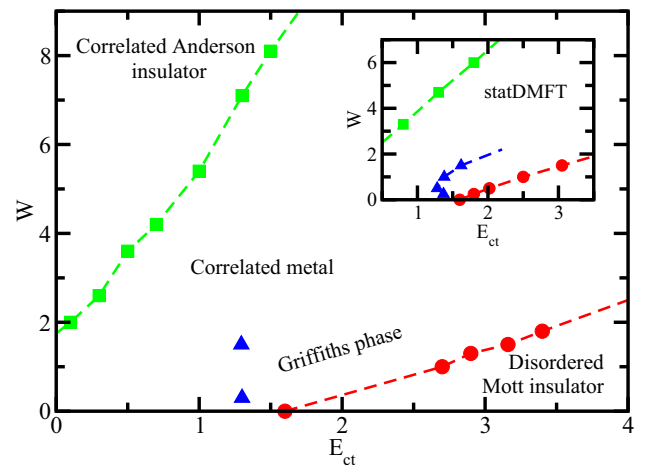


FIG. 1. (Color online) Phase diagram of the disordered CT model obtained within TMT-DMFT. $E_{ct} = -E_f$ is the CT energy and plays the role of the Hubbard U . For comparison, the inset reproduces the results obtained within *statDMFT* and presented in Ref. [14].

comparing the results in the main panel of Fig. 1 with those in the inset, we can see that in the case of the Mott-like transition TMT-DMFT predicts the phase boundary in very good agreement with *stat*DMFT. For the Anderson transition, according to TMT-DMFT a slightly larger amount of disorder than that observed in *stat*DMFT is necessary to drive the transition.

In the following, we look at how the order parameter and other physical quantities behave as the transitions are approached.

A. Disorder-driven transition

1. Critical behavior of the local density of states

Figure 2 shows the typical LDOS for conduction electrons at the Fermi energy as the disorder-driven transition is approached for different values of the CT energy. As expected, $\rho_c^{\text{typ}}(\omega = 0)$ decreases from the clean value as W increases due to disorder-induced localization effects. The typical LDOS for conduction electrons corresponds indeed to an order parameter within TMT-DMFT: Its vanishing defines the critical disorder at which the MIT takes place. In the present case, for all values of E_{ct} , $\rho_c^{\text{typ}}(\omega = 0)$ is seen to go to zero continuously as the MIT is approached, in agreement with *stat*DMFT results [14].

A detailed comparison to *stat*DMFT results for $E_{ct} = 1.3$ can be seen in Fig. 3. In accordance with the phase diagram of Fig. 1, within TMT-DMFT the transition is seen at a larger W value than within *stat*DMFT. Although in the present treatment the bath fluctuates from site to site—note that the bath given by Eq. (4) does depend on the site j , our results in Fig. 3 may suggest that not all the fluctuations induced by Anderson localization effects are captured by the simple TMT-DMFT treatment. Still, the behavior of the typical (and the inverse of average) LDOS is very similar in both treatments, allowing us to conclude that TMT-DMFT does give a reasonable picture of the transition. In addition, as pointed out before, since TMT-DMFT is numerical and analytically simpler than *stat*DMFT, it facilitates the understanding of the physics behind the problem we are looking at, as we discuss in this paper for the CT model.

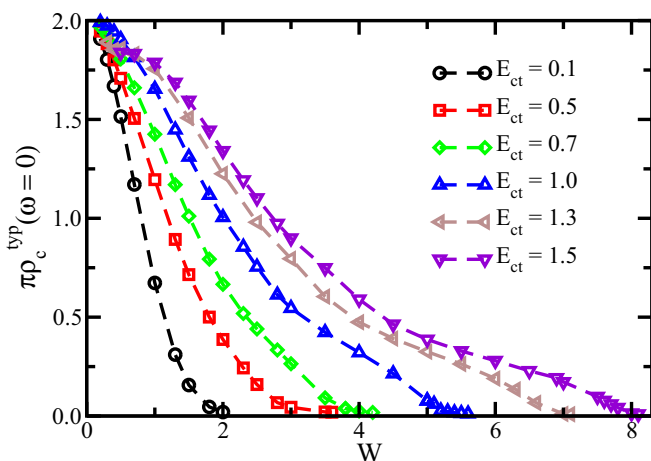


FIG. 2. (Color online) Typical values of the LDOS for conduction electrons at the Fermi energy as a function of the disorder strength W for different values of the CT energy E_{ct} obtained within TMT-DMFT.

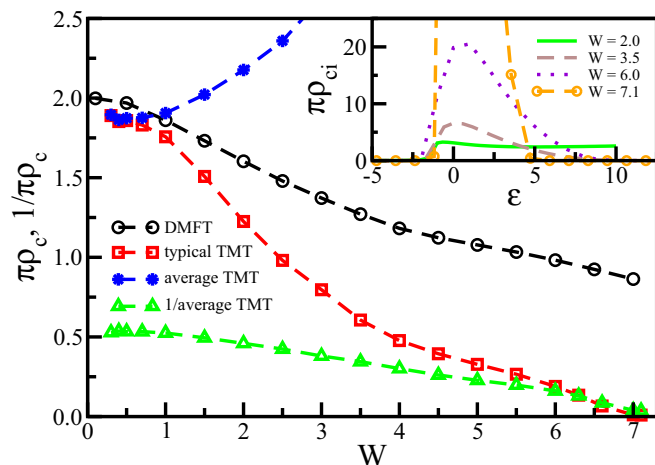


FIG. 3. (Color online) Comparison between TMT-DMFT and *stat*DMFT: Results are shown for the typical and 1/average values of the LDOS for conduction electrons at the Fermi energy obtained for $E_{ct} = 1.3$ and different values of the disorder strength, W . The inset shows the typical values of the QP weight Z as a function of W for both treatments.

In Fig. 4 the behavior of the typical LDOS is compared to that of the (arithmetic) average LDOS. It is interesting to note that, as it is the general case for *stat*DMFT results [9,14] (see also Fig. 3), within TMT-DMFT the *inverse* of the average LDOS goes to zero at the same disorder at which $\rho_c^{\text{typ}}(\omega = 0)$ vanishes. Figure 4 also shows the results of the standard DMFT calculation, where disorder is treated as in the coherent potential approximation (CPA), being unable to describe Anderson localization effects.

2. Statistics of local quasiparticle parameters

Let us now look at the properties of the single-impurity problems into which the lattice Hamiltonian is mapped. The inset of Fig. 4 shows the LDOS for each single-impurity of the

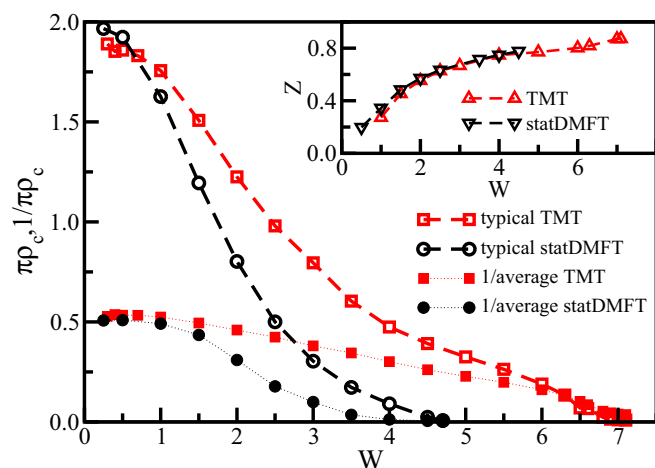


FIG. 4. (Color online) Comparison between TMT-DMFT and standard DMFT: Results are shown for the typical and average values of the LDOS for conduction electrons at the Fermi energy obtained for $E_{ct} = 1.3$ and different values of the disorder strength W . The inset shows the TMT-DMFT LDOS corresponding to each single-impurity problem as a function of the on-site energy ϵ .

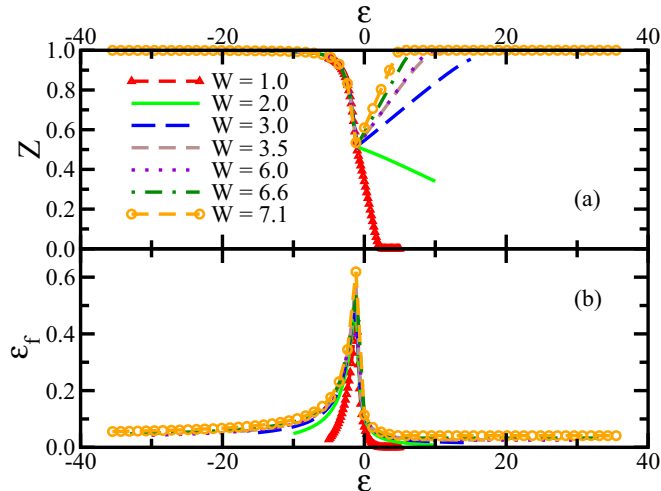


FIG. 5. (Color online) (a) Quasiparticle weight Z and (b) renormalized energy ε_f as a function of the on-site energy ε as the transition is approached (increase of W), for $E_{ct} = 1.3$. The results were obtained using TMT-DMFT.

ensemble, which is given by Eq. (7) and from which the TMT-DMFT results in the main figure are calculated. The conduction electrons, whose LDOS we are analyzing, see the f electrons through the function $\Phi(i\omega)$ [see Eq. (8)], which we can identify as an effective disorder potential. According to Eq. (14), $\Phi(i\omega)$ is written in terms of the two Fermi liquid parameters Z and ε_f . To understand the behavior of the LDOS close to the transition, below we present and analyze the results for these two parameters.

Figure 5(a) shows the behavior of the QP weight Z_j as a function of the on-site energy ε_j as disorder increases for $E_{ct} = 1.3$ (the same parameter of Figs. 3 and 4). For the smallest W considered, the values of Z_j are small (there are even sites with $Z_j \rightarrow 0$); as disorder increases the values of Z_j increase since the system tends to have most of the sites with $Z_j = 1$ (we know [9] that a “pure” Anderson insulator has all sites with $Z_j = 1$). The site with $\varepsilon = E_f = -E_{ct}$ is a special one: it corresponds to $n_c = n_f = 0.5$, which implies in $Z = 0.5$, as $Z_j = 1 - n_{fj}$ within SB. As a consequence of the presence of this site, close to the transition most of the sites have $Z_j = 1$, but some of them have $0.5 \leq Z_j < 1$. Note that none form local moments ($Z_j = 0$), a situation completely different than the one we will analyze in Sec. IIIB2 below.

The typical values of Z corresponding to the results in Fig. 5(a) are compared to the *statDMFT* results in the inset of Fig. 3. In the region where both treatments predict the system to be metallic, although the typical LDOS is larger within TMT-DMFT than within *statDMFT*, the typical values of Z practically coincide.

The results for the second SB parameter—the renormalized energy ε_{fj} —are shown in Fig. 5(b). This quantity is maximum for $\varepsilon_j = E_f = -E_{ct}$ and is relatively small for the majority of the sites, which correspond indeed to the intermediate to large $|\varepsilon_j|$ sites that have $Z_j = 1$ close to the transition.

But which mechanism of localization dominates the current MIT? In the case of the CT model, we have two kinds of electrons, localized or f electrons and conduction or c electrons. Within the SB method we consider $Z_j = 1 - n_{fj}$

and, for the CT model, $\langle n_{cj} \rangle + \langle n_{fj} \rangle = 1$. According to the above, most of the sites have $Z_j = 1$ (and small ε_{fj}) close to the MIT. $n_{fj} = 0$ for these sites, corresponding to electrons occupying c states, which are known to localize as disorder increases. Indeed, $\rho_{cj}(\omega = 0) \sim 0$ for these sites, as one can see in the inset of Fig. 4. Thus, as the transition is approached, most of the sites go through an Anderson type of localization. In other words, in the present case it is the Anderson mechanism for localization that is responsible for driving the system as a whole through the MIT.

If we now compare the results in Fig. 5 for $W = 3.5$ and $W = 6.0$, we see that Z_j and ε_{fj} coincide in the range of ε_j values present for both disorder strengths (the range of ε_j is, of course, larger for $W = 6.0$ than for $W = 3.5$), although $\rho_{cj}(\omega = 0)$ do change in this interval, as can be seen in the inset of Fig. 4. Note, however, that the rate at which the typical DOS decrease is smaller in the region where Z_j and ε_{fj} coincide than it is the case for smaller W values. By looking at the different quantities that determine $G_{cj}(\omega = 0)$ [see Eq. (8)], the results in Fig. 5 suggest that it is the bare disorder (ε_j) itself, rather than the scattering coming from the f electrons through $\Phi_j(\omega = 0)$, which dominates the behavior of the LDOS as the disorder driven transition is approached within TMT-DMFT.

To finish this section, the situation described here can be compared to that observed within TMT-DMFT for the Hubbard model [17], where close to the transition the sites have either $Z_j = 1$ or $Z_j = 0$, corresponding to electrons going through Anderson or Mott localization, respectively. (Note that the dependence of the LDOS for conduction electrons on Z is different in the two models considered.) In the current case, we do not have sites going through Mott localization ($Z_j = 0$): according to Fig. 5(a), the majority of the them have $Z_j = 1$, while a finite fraction has $0.5 \leq Z_j < 1$. For the latter $n_{fj} \neq 0$, that is, the occupation of *strongly correlated* f electrons is different from zero for these sites. Thus, although we do not have Mott-localized sites, because of the presence of the $0.5 \leq Z < 1$ sites, the current situation is also different than that in the noninteracting limit (where *all* sites have $Z_j = 1$), and a *correlated* Anderson insulator is present in the CT model phase diagram.

After discussing the results for the disorder-induced transition, in the next section we focus on the Mott-like transition.

B. Interaction-driven transition

1. Critical behavior of the local density of states

Figure 6 shows the typical LDOS for conduction electrons at the Fermi energy as the Mott-like transition is approached for intermediate values of disorder. A nonmonotonic behavior is observed, implying in an initial increase of the system “conductivity” when E_{ct} increases, which suggests that the disorder potential is *screened* by the correlation effects considered to exist between f electrons. This nonmonotonic behavior is in agreement with the *statDMFT* results we presented recently [14]. Indeed, in the current case the screening is stronger than within *statDMFT*—see, for example, the detailed comparison between TMT-DMFT and *statDMFT* presented in Fig. 7 for $W = 1.5$. Although strong, here the screening is not perfect and ρ_{typ} does not reach the value corresponding to the clean

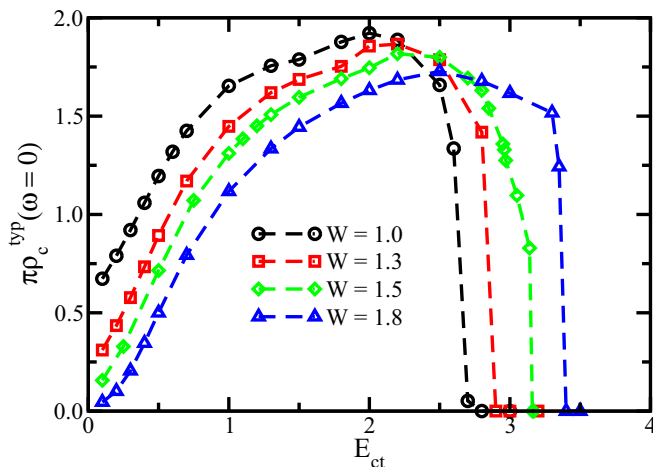


FIG. 6. (Color online) Typical values of the LDOS for conduction electrons at the Fermi energy as a function of the CT energy E_{ct} for different values of the disorder strength W , obtained within TMT-DMFT.

limit, as it is the case for the Hubbard model within DMFT [27] and TMT-DMFT [17].

Probably as a consequence of the strong disorder screening discussed above, the typical DOS within TMT-DMFT is seen to present a jump at the transition (see Figs. 6 and 7). This is in disagreement with *stat*DMFT for the CT model, which predicts that the order parameter vanishes continuously as the transition is approached [14]. Note, though, that according to Fig. 7 a good agreement is observed between the two calculations concerning the overall behavior of the typical and inverse of average LDOS, as well as the E_{ct} value at which the transition takes place (see also Fig. 1). Although the current results suggest that TMT-DMFT does not completely describe Anderson localization effects, which were shown to be responsible for the critical behavior also in the vicinity of the Mott-like transition [14], we can say that it does give a reasonable picture of it.

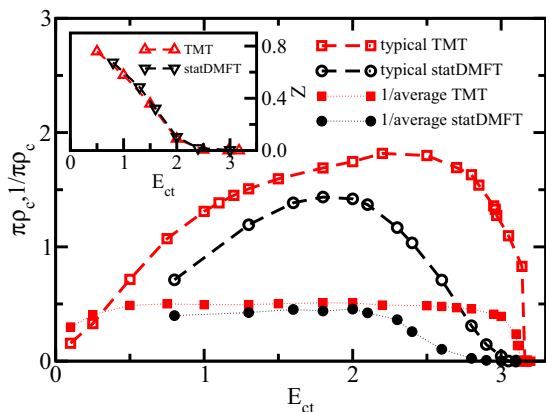


FIG. 7. (Color online) Comparison between TMT-DMFT and *stat*DMFT: Results are shown for the typical and 1/average values of the LDOS for conduction electrons at the Fermi energy obtained for $W = 1.5$ and different values of the CT energy, E_{ct} . The inset shows the typical values of the QP weight Z as a function of E_{ct} for both treatments.

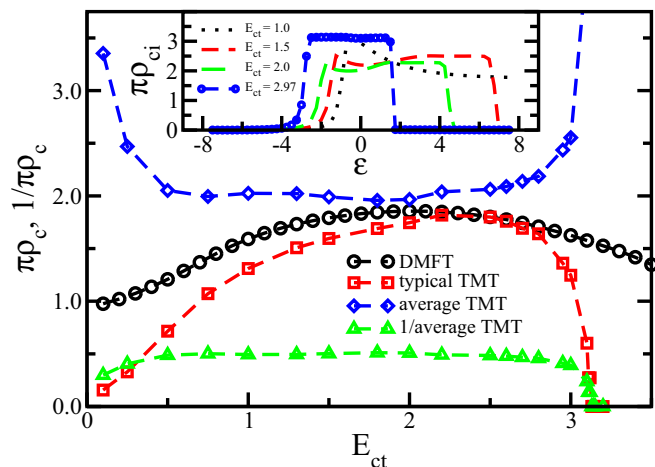


FIG. 8. (Color online) Comparison between TMT-DMFT and standard DMFT: Results are shown for the typical and average values of the LDOS for conduction electrons at the Fermi energy obtained for $W = 1.5$ and different values of the CT energy, E_{ct} . The inset shows the TMT-DMFT LDOS as a function of the on-site energy ϵ corresponding to each single-impurity problem.

To complete the discussion on the LDOS results, in Fig. 8 we compare the typical and average values of the LDOS obtained within TMT-DMFT to those valid within standard DMFT for $W = 1.5$ (the same parameter as Fig. 7). As it is the case for the disorder-induced transition (see Fig. 4), here the inverse of the average LDOS within TMT-DMFT is seen to vanish together with the typical LDOS. Also, standard DMFT average LDOS remains finite at the critical E_{ct} predicted by TMT-DMFT.

2. Statistics of local quasiparticle parameters

As we did in the previous subsection, we now look at the properties of the single-impurity problems, with the goal of understanding which sites of the ensemble dominate the behavior of the LDOS in the critical region. Figure 9(a) shows the QP weight Z_j for each single-impurity problem of the ensemble, for fixed disorder ($W = 1.5$), as the Mott-like transition is approached. As we can see, as E_{ct} increases, the large ϵ_j sites start to have $Z_j = 0$; as E_{ct} increases even further, more sites present $Z_j = 0$, while the region of sites with $Z_j \neq 0$ ($0 < Z_j < 1$ indeed) shrinks to the left of the figure. Very close to the transition all sites with positive ϵ_j , as well as few with $\epsilon_j \lesssim 0$, have $Z_j = 0$. Correspondingly, the typical value of Z decreases as the transition is approached, in very good agreement with *stat*DMFT, as can be seen in the inset of Fig. 7. Regarding the renormalized energy, which is shown in Fig. 9(b), we can see that the sites that form local moments ($Z_j = 0$) close to the transition are completely screened ($\epsilon_{fj} = 0$). For the rest of the sites, ϵ_{fj} presents a nonmonotonic behavior: it is finite for intermediate, negative values of the bare energy and tends to zero for the smallest ϵ_j considered.

To understand the results described above, let us first analyze the clean limit. In this case, DMFT maps the lattice problem onto only one single-impurity problem—that with $\epsilon = 0$, which has to satisfy $n_c + n_f = 1$, within the CT model.

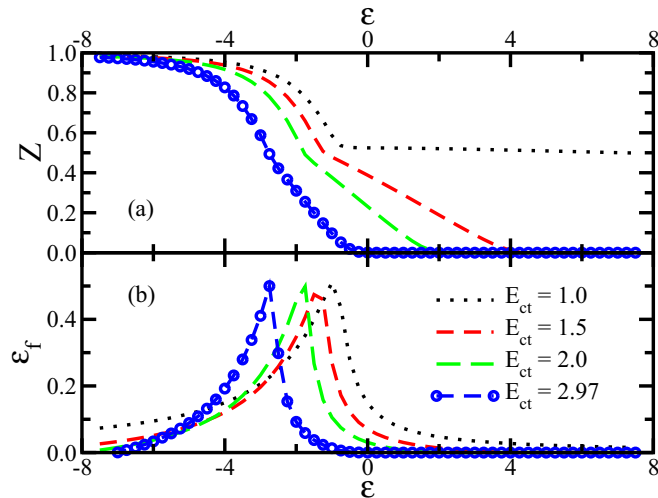


FIG. 9. (Color online) (a) Quasiparticle weight Z and (b) renormalized energy ϵ_f as a function of the on-site energy ϵ as the transition is approached (increase of E_{ct}), for $W = 1.5$. Results were obtained using TMT-DMFT.

The Mott transition is approached as $E_f = -E_{ct}$ decreases, which favors the occupation of the *localized* f level, implying in a decrease of the occupation for conduction electrons, n_c ; the transition happens when $n_c = 0$. Within the SB method, $Z = 1 - n_f$, which means that $Z \rightarrow 0$ as the transition is approached. As disorder is turned on, an ensemble of single-impurity problems has to be solved; close to the MIT transition, not all sites, but most of them, including those around $\epsilon_j = 0$ (the one that remains in the clean limit), have $Z_j \rightarrow 0$, as can be seen in Fig. 9(a). These sites go through the Mott mechanism for localization; as they are the majority in the present case, we conclude that Mott localization dominates the MIT that happens as the CT energy increases.

The current situation is different than that observed for the Hubbard model within TMT-DMFT [17]. In that case *all* sites turn to local moments as the transition is approached, in contrast to the present case where there exist sites with $0 < Z_j < 1$. Because of the presence of the $Z_j \neq 0$ sites, the insulating phase we observe here corresponds to a *disordered* Mott insulator.

C. Griffiths phase

Besides giving a good description of the MIT, TMT-DMFT is also able to describe the emergence of a Griffiths phase inside the disordered metallic region. This is possible by considering a Gaussian distribution of the on-site energy, as suggested in Ref. [23] and summarized by us in Sec. II.

To study the Griffiths phase, we focus on the behavior of Z for small disorder. In addition, instead of looking at its behavior as a function of ϵ , as we did above, we look at the evolution of its distribution $P(Z)$. In Fig. 10 we have the results for fixed CT energy $E_{ct} = 1.3$. As disorder increases, the distribution moves to smaller values of Z . More importantly, it develops a tail that follows a power law of the form

$$P(Z) \sim Z^{\alpha-1}, \tag{15}$$

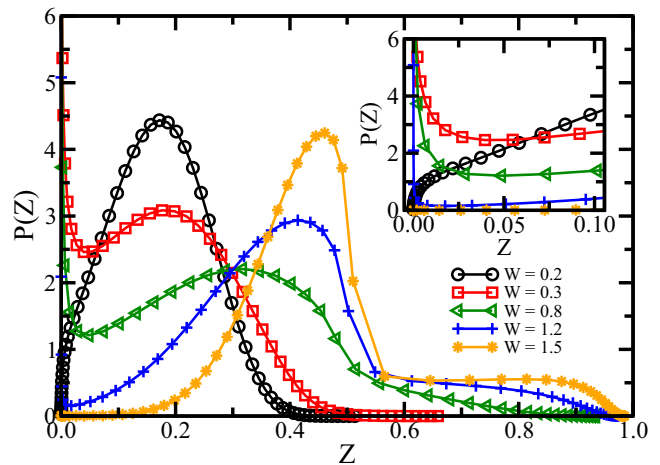


FIG. 10. (Color online) Distribution of Z obtained within TMT-DMFT as disorder increases for $E_{ct} = 1.3$. The inset highlights the fact that $P(Z = 0)$ becomes different from zero for intermediate values of disorder, which gives rise to a Griffiths phase in this range of parameters.

which is better visualized in Fig. 11. The exponent α is found by fitting the numerical data to the above equation; the values obtained in the present case of $E_{ct} = 1.3$ are shown in the inset of the figure. As we can see, α is a continuous function of W , becoming smaller than 1 for $W \sim 0.3$ in the current case. As a consequence of $P(Z)$ following a power law with $\alpha < 1$ (in some range of W), the system susceptibility and specific heat divided by the temperature T diverge in the low T limit (see Ref. [22] for a detailed discussion on this). This characterizes a Griffiths phase with non-Fermi liquid behavior.

According to the results in Fig. 10, as disorder increases even further, $P(Z)$ moves to larger values of Z and the low Z tail disappears. To precisely determine at which disorder the Griffiths phase terminates for $E_{ct} = 1.3$, one has to explore it in more detail, for example, by performing the current analysis

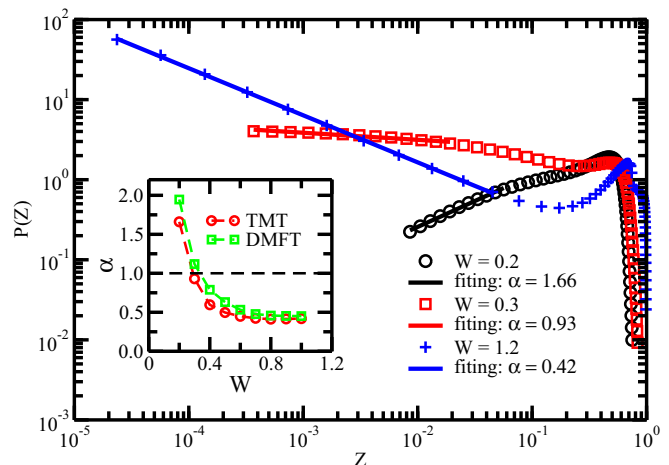


FIG. 11. (Color online) Distribution of Z and respective fits to a power-law observed within TMT-DMFT for $E_{ct} = 1.3$ and three values of W . The inset presents the power-law exponent α as a function of disorder, both within TMT-DMFT (as those in the main panel) and standard DMFT (not shown).

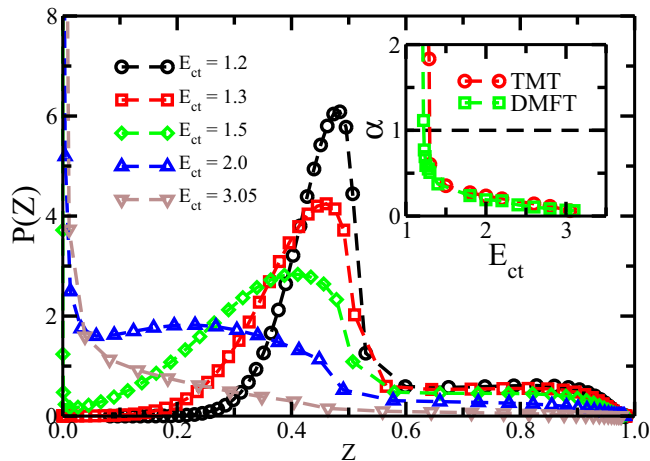


FIG. 12. (Color online) Distribution of Z obtained within TMT-DMFT as the CT energy increases, for $W = 1.5$. The inset presents the power-law exponent α as a function of the CT energy obtained within TMT-DMFT (main panel) and standard DMFT (not shown).

as a function of E_{ct} for different, fixed W . This is illustrated below for one fixed value of W .

Figure 12 shows the distribution of Z (main panel) and corresponding α (inset of the figure) for $W = 1.5$. As E_{ct} increases, $P(Z)$ moves to smaller values of Z . In the present case, α becomes smaller than 1 and the system enters the Griffiths phase for $E_{ct} \sim 1.3$. Differently than the previous case, here $P(Z)$ moves to even smaller values of Z , with α decreasing to zero, as the Mott-like transition is approached. Note that the E_{ct} we have just found for the onset of the Griffiths phase for $W = 1.5$ corresponds to the E_{ct} analyzed in Figs. 10 and 11; we can thus conclude that for $E_{ct} = 1.3$ the Griffiths phase is observed between $W \sim 0.3$ and $W \sim 1.5$.

The results in these three figures indicate that within TMT-DMFT the range of W and E_{ct} for which $\alpha < 1$ corresponds to the existence of a Griffiths phase in the region just preceding the Mott transition. This region is signaled in the phase diagram of Fig. 1 and is in accordance with *statDMFT* results for the same model (see Ref. [14] and also the inset of Fig. 1). A similar behavior has also been observed within *statDMFT* for the two-dimensional Hubbard model [10].

To finish, in the insets of Figs. 11 and 12, we compare the results obtained for α using TMT-DMFT [corresponding to $P(Z)$ in the respective main panels] and standard DMFT.

A Gaussian distribution of disorder is used in the two calculations. In both figures, in the range of the parameters shown, a very good agreement is seen between the two treatments considered. Note, however, that standard DMFT agrees well with TMT-DMFT concerning the *onset* of the Griffiths phase, but not its *extension*, as the former does not give a good prediction for the critical E_{ct} and W values at which the transitions take place, as previously shown in this paper.

IV. CONCLUSION

In this paper we solve the disordered charge-transfer model (CT) by using an extension of dynamical mean-field theory able to describe Anderson localization effects. In general, our results compare surprisingly well with those previously obtained by two of us using the *statDMFT* treatment [14]. The current calculation is simpler than the previous one, allowing us to better characterize the system when the metal-insulator transition is approached. Our results show, in particular, that as the interaction-induced transition is approached, a fraction of sites turn into local moment, but *not all* of them do it; this means that the corresponding insulating phase is a *disordered* Mott insulator. In the case of the transition due to disorder, most of the sites Anderson-localize; some of the correlated sites, though, remain occupied, corresponding to the presence of a *correlated* Anderson insulator in the phase diagram of the CT model.

In addition, according to our current TMT-DMFT results, the inverse of the arithmetic local density of states (DOS) is seen to vanish precisely at the disorder or interaction value at which the typical local DOS goes to zero, which indeed determines where the transition takes place. Exactly the same behavior is observed within *statDMFT* [9, 14], but an explanation for it is yet not known. The fact that the current treatment, which is analytical and numerically simpler than *statDMFT*, does show this behavior opens the possibility of understanding it, which is left as a direction of work to follow in the future.

ACKNOWLEDGMENTS

This work was supported by CAPES (W.S.O.), CNPq, and FAPEMIG (M.C.O.A.) and NSF Grant No. DMR-1005751 (V.D.).

-
- [1] A. M. Finkel'stein, Zh. Eksp. Teor. Fiz. **86**, 367 (1984) [Sov. Phys. JETP **59**, 212 (1984)].
 - [2] A. M. Finkel'stein, Z. Phys. B **56**, 189 (1984).
 - [3] C. Castellani, C. DiCastro, P. A. Lee, and M. Ma, Phys. Rev. B **30**, 527 (1984).
 - [4] C. Castellani, G. Kotliar, and P. A. Lee, Phys. Rev. Lett. **59**, 323 (1987).
 - [5] E. Miranda and V. Dobrosavljevic, Rep. Prog. Phys. **68**, 2337 (2005).
 - [6] E. Abrahams, S. V. Kravchenko, and M. P. Sarachik, Rev. Mod. Phys. **73**, 251 (2001).
 - [7] P. Dai, Y. Zhang, and M. P. Sarachik, Phys. Rev. B **45**, 3984 (1992).
 - [8] A. Georges, G. Kotliar, W. Krauth, and M. J. Rozenberg, Rev. Mod. Phys. **68**, 13 (1996).
 - [9] V. Dobrosavljević and G. Kotliar, Phys. Rev. Lett. **78**, 3943 (1997).
 - [10] E. C. Andrade, E. Miranda, and V. Dobrosavljevic, Phys. Rev. Lett. **102**, 206403 (2009).
 - [11] E. C. Andrade, E. Miranda, and V. Dobrosavljevic, Phys. Rev. Lett. **104**, 236401 (2010).
 - [12] D. Semmler, J. Wernsdorfer, U. Bissbort, K. Byczuk, and W. Hofstetter, Phys. Rev. B **82**, 235115 (2010).

- [13] D. Semmler, K. Byczuk, and W. Hofstetter, *Phys. Rev. B* **84**, 115113 (2011).
- [14] M. C. O. Aguiar and V. Dobrosavljević, *Phys. Rev. Lett.* **110**, 066401 (2013).
- [15] V. Dobrosavljević, A. A. Pastor, and B. K. Nikolić, *Europhys. Lett.* **62**, 76 (2003).
- [16] K. Byczuk, W. Hofstetter, and D. Vollhardt, *Phys. Rev. Lett.* **94**, 056404 (2005).
- [17] M. C. O. Aguiar, V. Dobrosavljevic, E. Abrahams, and G. Kotliar, *Phys. Rev. Lett.* **102**, 156402 (2009).
- [18] G. R. Stewart, *Rev. Mod. Phys.* **56**, 755 (1984).
- [19] G. R. Stewart, *Rev. Mod. Phys.* **73**, 797 (2001).
- [20] B. Shklovskii and A. Éfros, *Electronic Properties of Doped Semiconductors* (Springer-Verlag, Berlin, 1984).
- [21] M. J. Hirsch, D. F. Holcomb, R. N. Bhatt, and M. A. Paalanen, *Phys. Rev. Lett.* **68**, 1418 (1992).
- [22] M. C. O. Aguiar, E. Miranda, and V. Dobrosavljević, *Phys. Rev. B* **68**, 125104 (2003).
- [23] D. Tanasković, E. Miranda, and V. Dobrosavljević, *Phys. Rev. B* **70**, 205108 (2004).
- [24] P. Coleman, *Phys. Rev. B* **35**, 5072 (1987).
- [25] J. Zaanen, G. A. Sawatzky, and J. W. Allen, *Phys. Rev. Lett.* **55**, 418 (1985).
- [26] G. Sordi, A. Amaricci, and M. J. Rozenberg, *Phys. Rev. B* **80**, 035129 (2009).
- [27] D. Tanasković, V. Dobrosavljević, E. Abrahams, and G. Kotliar, *Phys. Rev. Lett.* **91**, 066603 (2003).
- [28] N. Read and D. M. Newns, *J. Phys. C* **16**, 3273 (1983).
- [29] E. Miranda, V. Dobrosavljević, and G. Kotliar, *J. Phys. Condens. Matter* **8**, 9871 (1996).